Macromolecules

ARTICLE

pubs.acs.org/Macromolecules

Connectivity and Structural Defects in Model Hydrogels: A Combined Proton NMR and Monte Carlo Simulation Study

Frank Lange,*,† Konrad Schwenke,‡,% Manami Kurakazu,§ Yuki Akagi,§ Ung-il Chung,§ Michael Lang,‡ Jens-Uwe Sommer,‡ Takamasa Sakai,§ and Kay Saalwächter*,†

†Institut für Physik — NMR, Martin-Luther-Universität Halle-Wittenberg, Betty-Heimann-Str. 7, D-06120 Halle, Germany

‡Leibniz-Institut für Polymerforschung Dresden, Hohe Strasse 6, 01069 Dresden, Germany

§Department of Bioengineering, School of Engineering, The University of Tokyo, 7-3-1 Hongo, Bunkyo-ku, Tokyo 113-8656, Japan

ABSTRACT: We present a study of the structure of Tetra-PEG model networks, using proton multiple-quantum NMR at low field in combination with computer simulations. Tetra-PEG is a novel high-performance hydrogel designed by combination of two symmetric tetra-arm macromonomers. In contrast to conventional hydrogels, which are highly heterogeneous due to fixed concentration fluctuations, Tetra-PEG exhibits a much less heterogeneous microstructure as indicated by previous light and small-angle neutron scattering studies. Here, the local-scale connectivity inhomogeneities, i.e., the sol and dangling polymer chains as well as the typical network connectivity defects resulting from the A—B reaction of four-arm macromonomers, are quantified experimentally for the first time, studying as-prepared Tetra-PEG hydrogels, cross-linked at different polymer concentrations and stoichiometries. To this end, we developed a novel approach for the analysis of double-quantum buildup curves consisting of well-distinguishable components with different segmental dynamic order parameters, benefitting from the superb large-scale homogeneity of the samples. As a model for each component we suggest different connectivity modes between the macromonomers—mainly regular single links and double links between individual stars as well as other network defects with lower order parameters. To support the model, we report results from computer simulations with the bond-fluctuation model, which confirm the concentration-dependent trends of the network and double-link fractions.

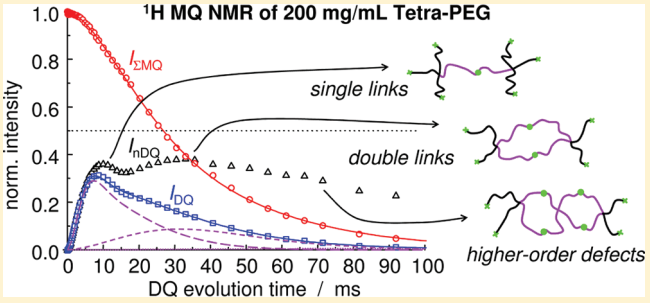

I. INTRODUCTION

Hydrogels are hydrophilic polymer networks swollen by water. The swelling equilibrium of uncharged hydrogels can be modeled by the Flory—Rehner theory[1] using expressions for the elastic forces of the polymer network chains and the osmotic forces of the solvent molecules as a function of the swelling degree. Both contributions are comparable at swelling equilibrium. Because of their absorption capacities, mechanical properties, and possible biocompatibility, (ionic) hydrogels are used as superabsorbers[2] and in biomedical materials.[3,4] Some hydrogel systems exhibit a stimulus-responsive volume phase transition due to a change of affinity of the polymer network chains to the solvent. This interesting property was discovered in the late 1970s[5] and finds applications in controlled drug delivery systems[6] and microfluidic devices.[7] Furthermore, we can distinguish between chemical or physical gels depending on the covalent or noncovalent origin of the cross-links.

The microscopic stucture of most polymer gels is clearly distinct from a homogeneous or regular network structure. The distribution of active strand lengths is typically not uniform, the topology is complex and disordered, the density of strands is subject to fluctuations, and the connectivity of the network junctions depends on their global embedding into the network structure. Additionally, networks made from most types of polymers will exhibit frozen density fluctuations of the chains. Any of these structural variations is frozen-in upon cross-linking of the polymer strands into an elastic soft solid, the gel.

In general, heterogeneities strongly affect the properties of the gel. For instance, the strain at break can be reduced, the equilibrium swelling ratio is increased, or the samples lose their transparency upon cross-linking. Heterogeneities can become visible upon swelling a gel as excess scattering at small angles. Light scattering experiments show intensity fluctuations ("speckle patterns") depending on the sample position,[8] and stretched gels exhibit an anomalous "butterfly pattern",[9] both indicating static density fluctuations of the polymer gel.[10] These static density fluctuations on length scales larger than the solution blob size have also been observed in computer simulations and were related to static density fluctuations of the active material inside the gel.[11]

Control of some of the structural heterogeneities previously mentioned can be attained by choosing particular precursor molecules as building blocks of the gel. For instance, end-linking of *f*-arm stars or linear chains via an *f*-functional cross-linker

Received: August 12, 2011
Revised: November 3, 2011
Published: November 21, 2011

allows to prepare gels of a homogeneous strand length between the junctions. Recently, Sakai and co-workers designed the Tetra-PEG hydrogel,[12] which is investigated in this article. An example for the particular properties of this gel is the breaking stress, which is in the order of MPa, i.e., 10−100 times higher compared to conventional hydrogels. The Tetra-PEG network is made of two different types of symmetric tetra-arm macromonomers: TAPEG, tetraamine-terminated poly(ethylene glycol), and TNPEG, tetra-NHS-glutarate-terminated PEG. In an A−B reaction the functional end-groups of TAPEG and TNPEG form covalent amide bonds in solution and *N*-hydroxysuccinimide (NHS) as side product. Of course, the A−B reaction pattern suppresses the formation of elastically inactive self-loops. As both macromonomers have approximately the same molecular weight (MW), the arm MW (1/4 of the star MW) and thus the molecular weight of the network chains M_c between the star centers (1/2 of the star MW) and therefore the cross-link density are well-defined. Interestingly, small-angle neutron scattering (SANS) experiments on as-prepared and swollen Tetra-PEG gels show no significant intensity upturn in the low q region,[13,14] however, clusters of PEG chains on length scales above 500 Å can be observed by static light scattering.[14]

We here extend these studies and apply solid-state NMR, which is a powerful technique to investigate the microstructure of polymeric networks,[15] as it gives direct access to fluctuations and local dynamic order phenomena in these systems. Popular methods are proton relaxometry studies by Hahn or solid echos,[16,17] deuterium NMR,[18,19] and ^{1}H multiple-quantum (MQ) NMR spectroscopy.[20−22] The latter has become a particularly valuable tool in the context of the characterization of polymer networks and entangled melts. Recent work on swollen networks include the study of swelling heterogeneities,[23] the actual gelation process,[24,25] solvent effects on the NMR observables,[26] and the structure of the poly(vinyl alcohol) cryo-hydrogels.[27]

In the present study, we apply low-field ^{1}H MQ NMR spectroscopy to analyze the network structure of as-prepared Tetra-PEG hydrogels in detail, focusing at molecular-level imperfections. Experimental parameters are the polymer concentration and the stoichiometry of the two macromonomers in the pregel solution. First, we deal with the fraction of dangling chain ends (unreacted arms) and sol chains. Second, we discuss the observation of network structural defects, i.e., multiple couplings of the four-arm macromonomers, and subsequently suggest a simple model to evaluate our experimental data. This evaluation is another showcase of the superb experimental capabilities of the MQ NMR technique. Extensive computer simulations using the bond-fluctuation model (BFM)[28,29] have been performed in order to compare the fraction of the network structure defects with the experimental findings.

II. METHODOLOGICAL BACKGROUND

Dynamic Order Parameter of Network Chain Segments. The main observable of the MQ NMR experiment is the local dynamic (time-averaged) order parameter of the polymer backbone S_b, which is defined by the square root of the plateau of the orientation autocorrelation function of the polymer chains (see ref 21 and references therein). This plateau is a result of the constrained chain dynamics in melts and networks. By making use of the orientation dependence of the dipolar coupling between different protons, ^{1}H NMR can be used to probe the plateau value of the orientation autocorrelation function. The backbone order parameter is in fact directly proportional to the time-averaged dipolar coupling strength, the residual dipolar coupling (RDC) constant D_{res} accessible by NMR. For bulk networks (elastomers) with N statistical segments between cross-links ($N \propto M_c$, the chains' MW) and neglecting the influence of entanglements,[30] we simply have $D_{res} \propto S_b \propto N^{-1} \propto M_c^{-1}$.

In swollen networks, however, the behavior of D_{res} becomes complex and solvent-dependent.[31] For a given network (fixed N) swollen to different degrees below equilibrium in θ solvent, D_{res} increases monotonically with increasing degree of swelling (decreasing polymer concentration c, since $Q = V/V_0 \propto c^{-1}$). This is simply due to the (ideally affine, but often subaffine) stretching of the chains. For chains swollen gradually in good solvent, however, D_{res} often decreases first before it eventually increases. We have shown that this can be explained by excluded-volume effects.[31] In the semidilute regime, the following general relation holds:

$$D_{res} \propto S_b \propto \frac{3}{5}\frac{l^2 R^2}{{R_0}^4} \tag{1}$$

where l is the segment length. R_0 is the equilibrium end-to-end distance of the chain in semidilute solution without stretching (equilibrated string of blobs), while R is the actual end-to-end distance in the swollen network subject to swelling-induced stretching. Assuming no stretching effect on R ($R = R_0$, which may hold in particular for low swelling due to topological "desinterspersion" rather than affine stretching), the excluded-volume effects lead to a swelling-dependent decrease according to

$$D_{res} \propto S_b \propto N^{-1} Q^{-1/4} \propto {M_c}^{-1} c^{1/4} \tag{2}$$

Ultimately at high swelling, the chains will stretch, leading to an upturn at higher Q (lower c). Irrespective of the exact nature of the swelling process (affine stretching vs subaffine desinterspersion), the RDC (order parameter) at swelling equilibrium is a well-defined quantity, following $D_{res,eq} \propto {Q_{eq}}^{-3/2} \propto {c_{eq}}^{3/2}$, as proven theoretically and confirmed experimentally.[31]

Our studied samples, having constant and known M_c, were cross-linked and measured at the same initial concentration c (as-prepared gels), and it was found experimentally that the polymer concentration at equilibrium swelling c_{eq} is about 1.2−2.2 times smaller than c over the investigated range of initial concentrations.[13] It is thus difficult to predict the actual dependence of D_{res} on c, as c does not represent a thermodynamically well-defined state.

^{1}H MQ NMR is a rather robust and quantitative tool for the analysis of the dynamics and structure in polymer networks and melts. Conceptual details on the use of MQ NMR to determine RDC constants and their distribution in networks can be taken from ref 21. We here just summarize the main issues necessary for the understanding of the data treatment. Essentially, different phase cycling schemes in the pulse sequence yield two time-dependent signal intensity functions, the double-quantum (DQ) buildup curve $I_{DQ}(\tau_{DQ})$ and the reference intensity $I_{ref}(\tau_{DQ})$, where τ_{DQ} is the variable length of the pulse sequence for multiple-quantum excitation and reconversion. I_{DQ} comprises the structural information on the polymer chains, that is, the residual dipolar coupling constant and its distribution. Yet, it also consists of contributions related to the overall decay of MQ coherences. This fact also applies to I_{ref} and this provides the opportunity to remove relaxation effects by a point-by-point

normalization

$$I_{nDQ}(\tau_{DQ}) = \frac{I_{DQ}(\tau_{DQ})}{I_{ref}(\tau_{DQ}) + I_{DQ}(\tau_{DQ}) - Be^{-\tau_{DQ}/T_2^*}} = \frac{I_{DQ}(\tau_{DQ})}{I_{\Sigma MQ}(\tau_{DQ})} \quad (3)$$

I_{nDQ} is the relaxation-free normalized DQ buildup curve, and $I_{\Sigma MQ}$ is the decay function of the total signal going through the different MQ coherences including modulated longitudinal magnetization. I_{nDQ} reaches a value of 0.5 relative to the total signal if $I_{\Sigma MQ}$ comprises all signal from the dipolar-coupled network components only. However, unmodulated longitudinal magnetization arising from non-network components leads to a slowly relaxing contribution to I_{ref}, which has to be subtracted before normalization. This is done by fitting the long-time tail of $I_{DQ} + I_{ref}$ to a singly (or sometimes doubly) exponential decay with the time constant T_2^* and the fraction B. Provided there is sufficient T_2 contrast, the non-network signal component can sometimes be disassembled into solvent signal and signal arising from sol and dangling chains, the latter having a shorter T_2^*.

Recently, Chassé et al.[32] introduced a novel and more precise function to obtain residual dipolar coupling constants from normalized DQ buildup curves. The empirical "Abragam-like" (A-l) function is able to overcome the validity limit of the inverse Gaussian function ($I_{nDQ} \leq 0.45$) so far used for fitting the buildup curves and is valid for networks with a high degree of homogeneity, i.e., with a very narrow distribution of D_{res}. It can thus be used as a Kernel function in the analysis of RDC distributions. Here, we extend the use of this function in order to fit I_{DQ} and $I_{\Sigma MQ}$ simultaneously. This becomes necessary because the hydrogels in question consist of fractions with very different D_{res} and, thus, very different apparent relaxation times reflected in $I_{\Sigma MQ}$ (for details see below). We thus have to consider the relaxation term, which is usually canceled by the normalization, more explicitly. We found that it can be described empirically by a stretched exponential function with a time constant τ and a stretching exponent β. The final fitting function, simultaneously applied to the two data sets, is

$$I_{DQ}(\tau_{DQ}) = \frac{A}{2}[1 - \exp(-(0.378 \cdot 2\pi D_{res}\tau_{DQ})^{1.5}) \times \cos(0.583 \cdot 2\pi D_{res}\tau_{DQ})] \exp[-(\tau_{DQ}/\tau)^{\beta}] \quad (4)$$

$$I_{\Sigma MQ}(\tau_{DQ}) = A \exp[-(\tau_{DQ}/\tau)^{\beta}] \quad (5)$$

Figure 1 demonstrates the successful use of eqs 4 and 5, as compared to the fits of I_{nDQ} with the inverse Gaussian function and the Abragam-like function for a highly homogeneous rubber sample. Below we will address its use in more inhomogeneous (multimodal) samples.

The **BFM** is a lattice Monte Carlo method to simulate polymers.[28] It takes only effective monomers into account, each of them representing several chemical monomers. A monomer on the lattice is represented by a cube occupying eight lattice points. Excluded volume is considered by the fact that each lattice site can only be occupied by one monomer. The bonds connecting the monomers have to be taken from a set of 108 vectors, which ensures together with excluded volume that bonds do not cross each other. The motion of the monomers is modeled by random jumps of a monomer to one of the neighboring lattice positions. A move is accepted if all sites of the new position are unoccupied and if the bonds connecting to the new position are still within the allowed set of bonds. The athermal solvent is considered implicitly by the empty lattice sites. Among many other applications, the BFM has been used to investigate the conformational properties of networks chains[33,34] and the dynamics of linear polymers in solution,[35] where for the latter the number of Monte Carlo steps can be associated with a reduced time variable.

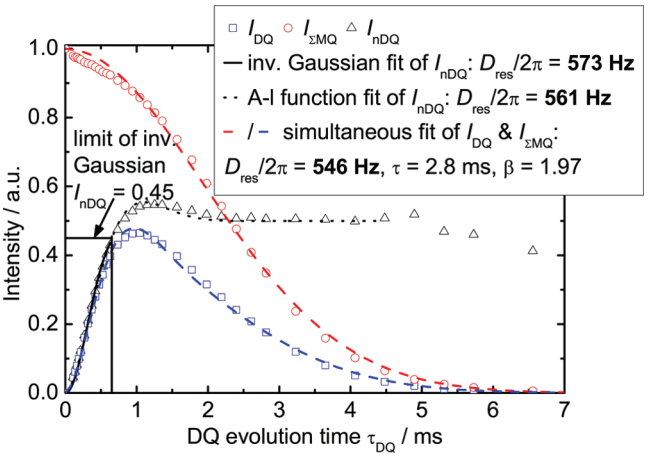

Figure 1. Exemplary MQ NMR buildup and decay curves of a highly homogeneous natural rubber. The sample was prepared by a conventional cure system (for details see ref 22), and the data were kindly provided by J. L. Valentín. $I_{\Sigma MQ}$ is obtained from the reference and DQ signal after tail subtraction (2.7%). I_{DQ} and $I_{\Sigma MQ}$ were renormalized to achieve $I_{\Sigma MQ}(0) = 1$. The fits with the inverse Gaussian (solid line), the A-l function (dotted), and eqs 4 and 5 (dashed) yield almost the same residual dipolar coupling constant.

III. EXPERIMENTAL SECTION

Tetra-PEG. TAPEG and TNPEG star polymers with a molecular weight of 10 kg/mol were prepared as previously reported.[12] Both polymers were dissolved in buffer solutions prepared with D_2O with polymer concentrations between 15 and 200 g/L. Gelation was initiated by mixing the TAPEG and TNPEG solutions in equal (stoichiometric, $r = 1$) or unequal (off-stoichiometric, $r = 11:9, ..., 3:1$) amounts. The pregel solution was filled into 10 mm OD NMR tubes. Care was taken regarding the maximum sample height of 1 cm to ensure homogeneity of the B_1 field in the NMR spectrometer. Sakai et al. have estimated the overlap concentration of TAPEG and TNPEG on the basis of the viscosity of the solutions, obtaining a value of about $c^*_{exp} \approx 60$ g/L.[12]

NMR Spectroscopy. The low-field NMR experiments were performed on a Bruker minispec mq20 with a magnetic field of $B_0 = 0.47$ T and 90° and 180° pulse lengths of 3 and 5.6 μs, respectively. The temperature was held at 40 °C by a BVT3000 operating on an air flow. Buildup curves of the longitudinal (T_1) relaxation were measured by a saturation recovery experiment with a variable relaxation delay. The pulse sequence for the MQ NMR experiment is described in detail in refs 21 and 24. The relaxation delay between the scans was chosen to be larger than $5T_1$ of the polymer ($T_1 \approx 0.6$ s). The solvent T_1 is much longer, thus, its relative amount is not determined quantitatively in this experiment (*vide infra*). Depending on the polymer concentration, the number of scans for each point in the MQ NMR experiment was between 32 and 512.

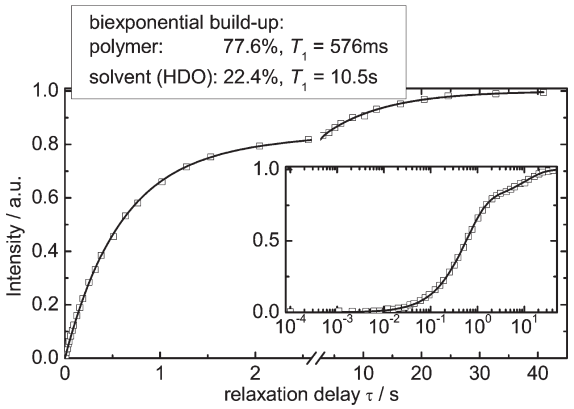

Figure 2. Buildup of the longitudinal magnetization for the 120 g/L stoichiometric Tetra-PEG sample measured by a saturation recovery experiment with variable relaxation delay τ. The solid line is a fit with the bimodal buildup function (7). The inset shows the same data on a logarithmic time scale.

BFM. Solutions of monodisperse star polymers with four arms were created at concentrations ranging from dilute solutions up to concentrated systems at ϕ = 0.5, comparable to polymer melts.[35] The arm length N_a of the stars varied from 4 to 64 monomers, and each star, i.e., its four end momomers, was randomly assigned to be either of type A or type B. The number of star polymers in the simulation box ranged from 1536 to 8192. The star solutions were equilibrated and then cross-linked. Whenever two free end monomers of different type hit each other, a new bond between them was formed. The reactions were continued until a conversion ratio of ~95% was reached. During the reactions, the buildup of the network structure was monitored by recording the newly formed bonds between the star arms. A connectivity analysis revealed the volume fractions of active and dangling gel molecules and the weight fraction of gel. Furthermore, the polymer volume fraction of dangling rings and multiple connections between molecules were determined. More details about the simulations are reported in a recent publication.[36] To compare the results of systems with different star sizes ($N = 4N_a$ monomers), we scaled the concentration with the (geometric) overlap concentration $c^*_{geom}(N)$, which is defined by

$$c^*_{geom} = \frac{3N}{4\pi {R_{g0}}^3} \tag{6}$$

where ${R_{g0}}^2 = (3 - 2/f)N_a l^2/6$ refers to the radius of gyration of the star polymers with functionality f (here 4) and segmental size l as determined at high dilution ($c \ll c^*_{geom}$).

IV. RESULTS AND DISCUSSION

Dangling and Sol Chain Content. In order to calculate the contribution of the highly mobile polymer chains according to eq 3, we have to consider the signal of the residual solvent protons (mainly HDO) in the sample. As there is no chemical shift resolution available with the low-field NMR equipment, the fraction of solvent signal can be determined by its longitudinal relaxation behavior. Figure 2 shows the buildup curve of the longitudinal magnetization measured by a saturation recovery experiment for the stoichiometric Tetra-PEG gel with a polymer concentraion of 120 g/L. Two components with very different relaxation times can be identified, and a fit using

$$I_{satrec}(\tau) = A_{poly}[1 - \exp(-\tau/T_{1,poly})] + A_{solv}[1 - \exp(-\tau/T_{1,solv})] \tag{7}$$

where

$$A_{poly} + A_{solv} = 100\% \tag{8}$$

yields the signal fractions and the relaxation times of the polymer and the solvent. The values of $T_{1,poly}$ are about 0.6 s for all samples, and $T_{1,solv}$ is always above 7 s.

As mentioned in the Experimental Section, the MQ NMR experiment was performed with a recycle delay of at least $5T_{1,poly}$. However, this also means that the experiment behaves as a T_1 filter for the solvent protons and the signal fraction obtained by long-time tail fitting of $I_{ref} + I_{DQ}$ is smaller than expected. The tail fitting is demonstrated in Figure 3a for the same sample. Unfortunately, due to missing T_2 contrast, we could not identify a second distinguishable exponential long-time decay, as commonly found in bulk elastomers.[27] We assume the tail fraction B to be a mixture of polymeric material with isotropic dynamics (sol and dangling chains) and the T_1-filtered signal of the solvent, which can be calculated from eq 7. To justify this assumption, we also plotted the tail fitting procedure for an off-stoichiometric Tetra-PEG network in Figure 3b. With the given experimental parameters, the contribution of solvent signal to B is calculated to be only 47% for the 3:1 sample, thus, the residual tail signal (52%) is ascribed to isotropically mobile (elastically inactive and sol) polymeric material. This plot also gives the impression that the fraction of active network chains in this sample (sloppily speaking, the magnitude of the DQ buildup curve I_{DQ}) is very low compared to the stoichiometric sample in Figure 3a. Finally, we can calculate the fraction of the isotropically mobile polymeric material with respect to the total polymer amount via

$$f_{sol+dangling} = \frac{B - A_{solv}[1 - \exp(-\tau_{rd}/T_{1,solv})]/I_{satrec}(\tau_{rd})}{A_{poly}} \tag{9}$$

where τ_{rd} is the recycle delay of the experiment. Figure 4a shows $f_{sol+dangling}$ as a function of the polymer concentration. This quantity is below 8% for all stoichiometric samples, and the lowest concentration of non-network defects can be found in the 60 g/L sample. However, we assume that our method still slightly underestimates $f_{sol+dangling}$ because we have to expect at least 7% of non-network defects, based upon the estimation of the activity of functional groups for TAPEG and TNPEG.[12] Nevertheless, this data gives the impression that the reaction turnover of the A−B reaction between the macromonomers is almost perfect, which supports the recent IR spectroscopic study by Akagi et al.[37]

The evaluation of $f_{sol+dangling}$ has been repeated for off-stoichiometric samples with r = [TAPEG]/[TNPEG] > 1 and different polymer concentrations. The results are shown in Figure 4b. As expected, the lack or excess of one of the two reagents results in an underdeveloped polymer network with a large amount of uncoupled and finite chains. This observation supports the findings reported by Sakai et al.,[12] i.e., a stoichiometric and symmetric gelation process yields networks with the best mechanical properties.

The alert reader might now suggest the application of the theory of Miller and Macosko[38] to estimate the reaction efficiency. If we consider the existence of structural network defects (multiple connections between two macromonomers, see Figure 6), which will be proven below, then one of Flory's ideal-network assumptions[1,38] is violated, namely "no intramolecular reactions occur in finite species". That is why the Miller−Macosko theory has to be refined for this case.[45]

Evaluation of the MQ NMR Buildup Curves. The data points obtained by the MQ NMR experiment for the sample with c = 120 g/L are plotted in Figure 5a. $I_{\Sigma MQ}$ and I_{DQ} have been

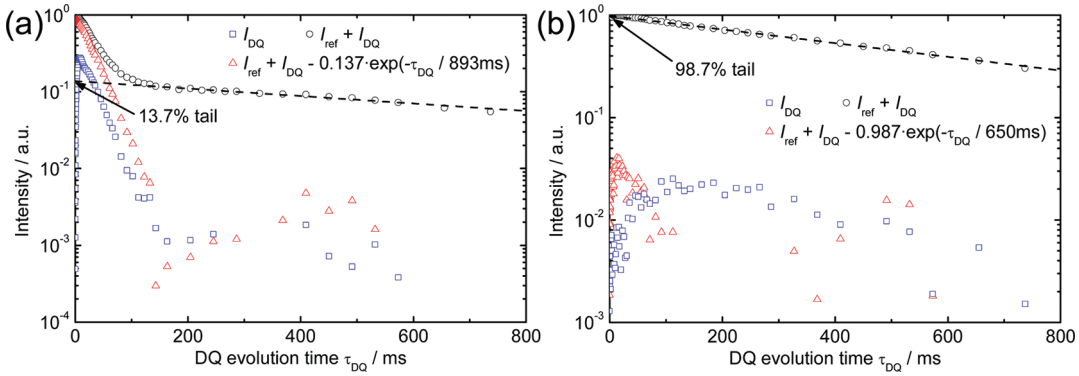

Figure 3. MQ NMR buildup and decay signals for (a) the 120 g/L stoichiometric and (b) the 40 g/L 3:1 off-stoichiometric Tetra-PEG samples plotted on a semilogarithmic intensity scale. The long-time tail fitting by an exponential decay is demonstrated. It yields the joint fraction B of non-network polymer chains and solvent signal.

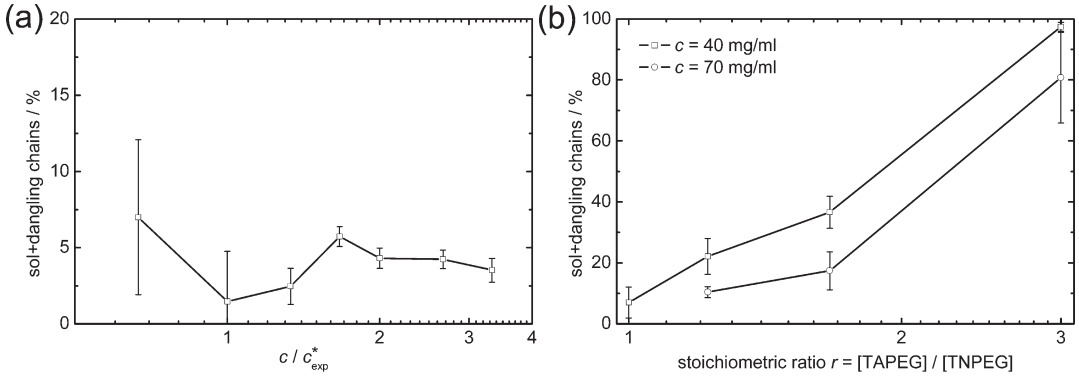

Figure 4. Fraction of the non-network polymer chains $f_{sol+dangling}$ according to eq 9 for (a) the stoichiometric samples as a function of the overlap ratio c/c^*_{exp} and (b) the off-stoichiometric samples as a function of the stoichiometric ratio.

renormalized by the same factor to achive $I_{\Sigma MQ}(0) = 1$ after the tail subtraction. For the normalized DQ buildup curve I_{nDQ}, we notice an anomalous behavior: It never reaches the value 0.5, and there appears to be a gradual buildup in three steps. The latter could be accounted by a superposition of multiple buildup curves, each with an individual residual dipolar coupling constant. If we assume such a superposition, we also have to expect different time constants $\tau(D_{res})$ in the relaxation term of each component, since their D_{res} is very different. These terms do not cancel by the point-by-point normalization, and I_{nDQ} does not reach 0.5 due to this additional dependence on τ_{DQ}, as seen in the following relation:

$$I_{nDQ}(\tau_{DQ}) = \frac{\sum_i a_i \tilde{I}_{DQ,i}(\tau_{DQ}) \exp[-(\tau_{DQ}/\tau_i)^{\beta_i}]}{\sum_i a_i \exp[-(\tau_{DQ}/\tau_i)^{\beta_i}]} \neq \frac{\sum_i a_i \tilde{I}_{DQ,i}(\tau_{DQ})}{\sum_i a_i} = \sum_i a_i \tilde{I}_{DQ,i}(\tau_{DQ}) \quad (10)$$

where we consider relaxation terms similar to eqs 4 and 5. $\tilde{I}_{DQ,i}$ is the relaxation-free DQ buildup curve of the ith component. The fractions of the components a_i are normalized to 1.

In order to extract information about the fractions a_i and the residual dipolar coupling constants $D^{(i)}_{res}$ from I_{DQ} and $I_{\Sigma MQ}$, we constructed the following simultaneous fitting function

$$I_{DQ}(\tau_{DQ}) = \frac{1}{2}\sum_{i=1}^{3} a_i[1 - \exp(-(0.378\cdot 2\pi D^{(i)}_{res}\tau_{DQ})^{1.5}) \times \cos(0.583\cdot 2\pi D^{(i)}_{res}\tau_{DQ})] \exp[-(\tau_{DQ}/\tau_i)^{\beta_i}] \quad (11)$$

$$I_{\Sigma MQ}(\tau_{DQ}) = \sum_{i=1}^{3} a_i \exp[-(\tau_{DQ}/\tau_i)^{\beta_i}] \quad (12)$$

assuming three buildup components, each with a vanishingly narrow D_{res} distribution. Two of them correspond to network structures, which will be discussed explicitly below. The third component sums up all defects that lead to corrections at the low order parameter wing of the distribution in order to obtain a stable fit of the second component. Equations 12 and 13 have 12 free parameters in total (11 formally independent ones, taking $\Sigma_i a_i = 1$), i.e., we have to expect several local minima for the error parameter χ^2. We therefore applied a simulated annealing algorithm,[39] followed by a Levenberg–Marquardt fit (Origin 7.5) to find the global minimum of χ^2. The resulting fit curves are plotted along with the data points and the residuals in Figure 5a. Additionally, we plotted each component of I_{DQ} for comparison with the "steps" observed in the normalized buildup intensity I_{nDQ}. Furthermore, Figure 5b shows the same data and fits on a logarithmic intensity scale. Unfortunately, this analysis is not

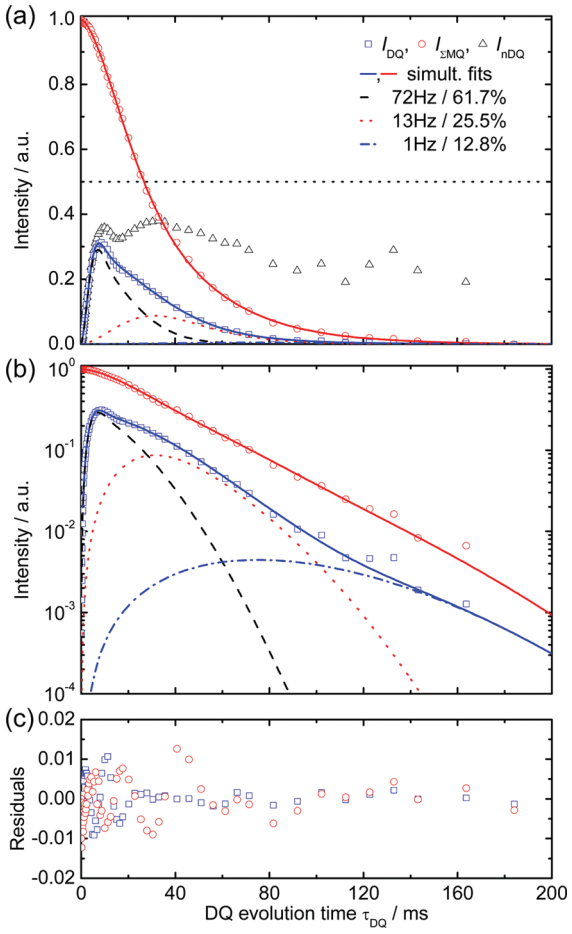

Figure 5. (a) Experimental data points for the DQ buildup I_{DQ} (squares) and the decay of the total MQ magnetization $I_{\Sigma MQ}$ (circles) for the 120 g/L stoichiometric Tetra-PEG sample. The normalized DQ intensity I_{nDQ} (triangles) has been calculated according to eq 3. The simultaneous fit by eqs 11 and 12 is demonstrated by the solid lines. Each component of I_{DQ} is drawn for further convenience. (b) shows the same data on a logarithmic intensity scale. Additionally, the residuals for the fit are plotted (c).

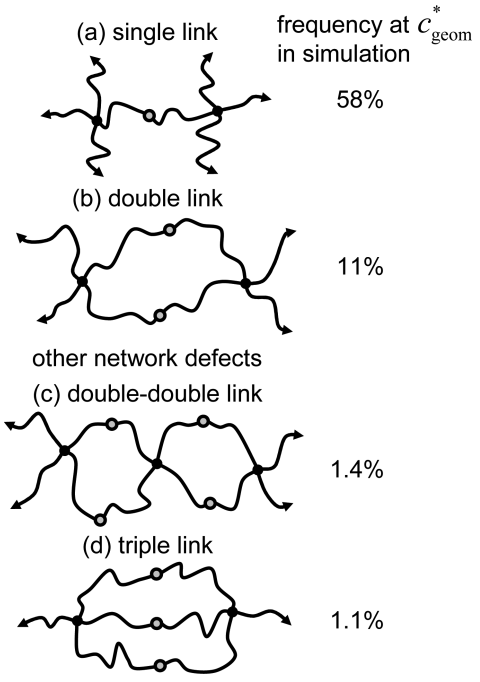

Figure 6. Schematic representation of possible connectivity structures formed by an A−B copolymerization of four-arm macromonomers including their frequency at c^*_{geom} in the BFM simulations. The single link (a) corresponds to the ideal state. The double-link (b) is by far the most frequent cyclic network defect of A−B networks at the concentrations of the present study.[45] (c) and (d) are examples of more complex network defects that possibly contribute to the low order parameter wing[36] and are accumulated in the third component of the fit function.

feasible for the off-stoichiometric samples due to the low signal-to-noise ratio of the DQ buildup function I_{DQ}. Also note that a large fraction of dangling chains (as in off-stoichiometric samples or at low degree of cross-linking) implies a broad distribution for the cross-link fluctuations. This leads to broadly smeared out peaks for any type of connection between stars.

Nature of Network Defects. Before discussing the actual amounts of network and defect fractions in the light of our computer simulation results, we first focus on the assignment of the three components found in the buildup curves. For an interpretation, we suggest the connectivity structures drawn in Figure 6. The component with the highest RDC constant $D^{(1)}_{res}$, i.e., the lowest chain molecular weight $M^{(1)}_c$ = 5 kg/mol, is the single link as it is expected to be present when a 4-functional macromonomer reacts with four different neighbors. Furthermore, we identify double connections between two neighboring macromonomers (Figure 6b) with the second component. This is the most simple (and most abundant) defect possible in networks formed by an A−B reaction. By counting the number of arms involved in this structure, we can get a rough estimation for the "apparent" molecular weight (i.e., the MW measured by the MQ NMR experiment) between the cross-link points: $M^{(2)}_c \approx x \cdot 2M^{(1)}_c$ with $2 \le x \le 3$. Since according to eq 2 $D^{(1)}_{res}/D^{(2)}_{res} = M^{(2)}_c/M^{(1)}_c$ at fixed concentration, a factor of 4−6 is thus expected for the RDC constants on the basis of the underlying fixed-junction model.

The third component cannot be associated with a single defect structure. It rather corresponds to a sum of higher-order defects with low orientational order, which will be designated as "other defects". Two examples are given in Figure 6c,d. We note that even for a well-defined chain length there is some distribution of order parameters because of the randomness of network connectivity. Therefore, a separation of various components is only possible if they are sufficiently resolved in the RDC distributions and have sufficient intensity. As a consequence, not all well-defined defect structures can be resolved (cf. Table 3 of ref 36), and our analysis is restricted to stoichiometric A−B networks at high conversion.

Figure 7 shows the RDC constants $D^{(i)}_{res}$ along with the fitting errors as a function of polymer concentration. The RDC constants depend on concentration, and somewhat unexpectedly, we observe different scaling exponents for the different components. As anticipated from the considerations under Methodological Background, the underlying physics is complex, and further theoretical work will be necessary to understand in particular the weakly positive and the comparably stronger, also positive concentration dependence of the RDC constants associated with primary network (single link) and the first-order defect (double link) fractions, respectively. Over the given range of concentrations, they are separated by a factor of about 4−8 upon

dx.doi.org/10.1021/ma201847v |*Macromolecules* 2011, 44, 9666–9674

decreasing c, which matches well with the simple prediction above.

It should be noted that a more precise calculation of the polymer backbone order parameter $S_b \propto M_{app}^{-1}$ will have to consider the end-to-end distance fluctuations of the polymer chains. According to the phantom model,[40,41] there is an interplay of two effects: the fluctuations of the network chain are reduced by the factor 1/2 due to the parallel chains, and the functionality of two cross-links reduces by 1 for the double link in Figure 6b. These two facts complicate the exact calculation of the order parameter. A more detailed assessment based on the phantom model is presented in our recent publication,[36] where we find only a factor of about 2 for the order parameter ratio between single and double links. Since in this work steric and excluded-volume effects were not taken into account, and only the bond vector rather than the tensor order parameter was considered (the latter reflecting the experimental RDC), all of which are known to affect the results,[26,31] further theoretical work will be necessary for a final interpretation of the experimental RDC constants.

Network defect structures have already been considered for a long time,[42,43] but to our knowledge, they have never been observed directly. It is notable that the primary network fraction and one well-separated defect fraction with distinct ("quantized") motional anisotropy could here be identified and characterized quantitatively for the first time. This becomes possible because of the superb homogeneous structure of the Tetra-PEG at larger length scales, rendering the two main components essentially narrowly distributed. This is the reason why for each fraction a single-component model represented by eqs 4 and 5 works so well. It is important to point out that networks in the vicinity of c^* are best suited for our analysis, since the fraction of double links is most significant.[45] Furthermore, the order parameters in networks at high concentration $c \gg c^*$ depend on entanglements.[30] This leads to an increasing overlap of the order parameter distributions of single and double links with increasing concentration, in agreement with simulation data[36] or Figure 8. Note that the problem of cyclic defects can be reduced to the determination of the frequency of a single cyclic defect, since there are unique relations between all cyclic defects in polymer networks.[45,46] Therefore, a well-defined experiment for the determination of one of these defects is of paramount importance for a quantitative analysis of network structure.

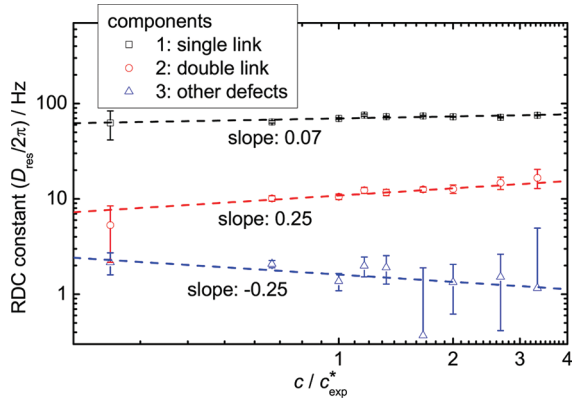

Figure 7. RDC constants obtained from the fit with eqs 11 and 12 for different polymer concentrations. The bars show the error values obtained from the Levenberg−Marquardt fit.

We can thus summarize that the statement of the "ideality" of the Tetra-PEG network with postulated diamond-like connectivity structure, as concluded indirectly from the lack of excess scattering of neutrons or light at low scattering angle in previous studies,[13,14,44] addresses only one facet of these fascinating systems, namely the (non)existence of strong frozen-in concentration fluctuations. Focusing on a more local level, the present study unveils substantial defect structures. It does not contradict the previous conclusion, but it emphasizes that from a topological point of view the Tetra-PEG is far away from an ideal or perfect network.

Fraction of Network Defects and Comparison with BFM Simulations. The signal (= weight) fraction of each component a_i was extracted from the fits with eqs 12 and 13. In order to verify the proposed model of the network structure defects, we performed large-scale BFM simulations.[36] The comparison of the concentration axes in experiment and simulation deserves some comments. First, the geometric overlap concentration c^*_{geom} defined by eq 6, which we can straightforwardly extract from the simulations, cannot be matched with the experimental c^*_{exp}, which is based on rheological observations. As to experimental chain dimensions, ref 13 gives a value of R_g = 28.6 Å under θ conditions, based on Gaussian statistics. All scattering data,[13,14] even for the fully swollen stars of 10 kDa, yield R_g < 20 Å. Thus, all "swollen" samples appear in fact collapsed. Because of these quantitative discrepancies, we cannot use the scattering data to match c/c^*.

As an alternative, the gel point concentration c_{gel} can also not be used for comparison, since it was again determined differently in

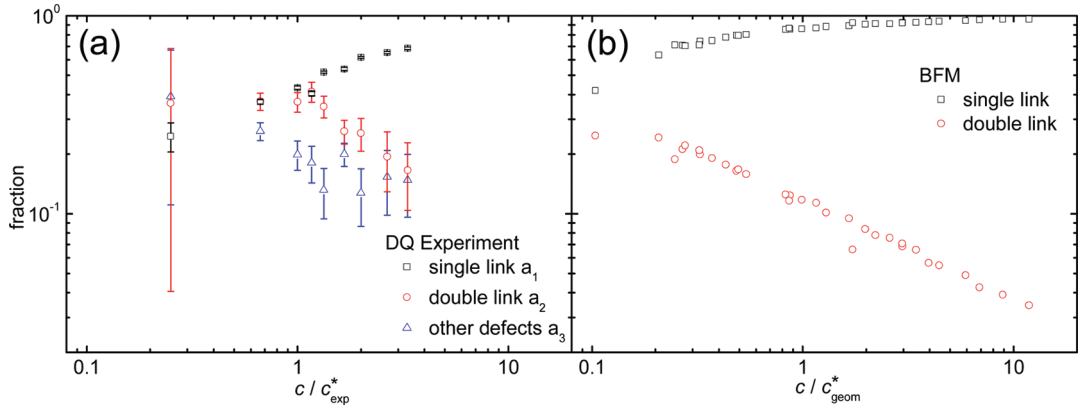

Figure 8. Fractions of the network structural defects considered in Figure 6. The experimental data, referenced to the rheological overlap concentration, are compared with the defects counted after the BFM simulation. The simulation data were referenced to the geometric overlap concentration.

experiments and simulations. In the former, a simple test identifying the gelled sample with the lowest possible concentration falls victim to a flocculation of stars (meaning increasing local concentration and liberation of excess solvent from the formed gel), while in the latter an extrapolation to the theoretically lowest concentration leading to a percolated structure was done, and no flocculation effects (leading to changes in local concentration) were observed.[36] Thus, at present we lack a proper, physically motivated way of comparing concentrations between experiments and simulations on the basis of the currently available data.

Figure 8 compares the fractions obtained from MQ NMR (a_1, a_2, and a_3) with the fraction of single and double links extracted from the BFM simulation. The concentration dependence of the amount of double links has been predicted theoretically,[36] in agreement with the simulation data that is shown in Figure 8b. Certainly, deviations in the theoretically and experimentally determined fractions may occur due to different solvent properties and chain conformations. The BFM simulation uses an athermal solvent, whereas the Tetra-PEG chains are enclosed by good solvent. Also, the polymers in both systems possess different characteristic ratios C_∞. Taken together, the probabilities of chains to "refold" and form rings are different at the same overlap ratio c/c^* in both systems.

Since the data from experiments and simulations follow the same trend, we take this as a good indication that our analysis indeed determines the fraction of double links in the networks. For the lowest concentrated gel measured in this study (c/c^*_{exp} = 0.25), we find a fraction of double links of 36%. This number drops off to about 17% for the most concentrated sample ($3.3c^*_{exp}$). For the other defects (a_3) we again find the highest fraction at a scaled c/c^*_{exp} = 0.25 (39%), and the lowest fraction at a scaled c/c^*_{exp} = 2 (13%), from where it appears to level off. We notice that the BFM simulation overestimates the single-link component (network fraction) and correspondingly underestimates the double links as compared to the experimental fractions. The fraction of the other defects is certainly subject to the largest possible systematic error in the multicomponent fitting. A direct comparison between this signal fraction and any particular defect structure determined after the BFM simulations is rather misleading because it always refers experimentally to a superposition of many kinds of structures. Note that the experimental and simulation data for the single and double links would in fact overlay if the overlap ratio of the latter would be multiplied by a factor of about 8, which is well within the range of the uncertainties of the different c^* definitions discussed above.

V. CONCLUSIONS

We performed low-field MQ NMR as well as Monte Carlo simulations to investigate the microstructure of the Tetra-PEG hydrogel, which is a network formed by an A−B reaction of two symmetric four-arm polymers. For the first time, we were able to experimentally quantify connectivity inhomogeneities in a polymer network, i.e., we determined the fraction of elastically inactive defects (dangling chains, loops, etc.) and, more importantly, the actual network fraction along with two well-separated populations of connectivity defects that are part of the network.

The fraction of non-network defects was found to be rather low for stoichiometric samples within the range of initial concentrations at preparation considered (15−200 g/L), proving a very high reaction turnover. As expected, a much larger amount of such defects was observed in off-stoichiometric gels.

Our central and new finding was a multiple-component behavior in the DQ buildup curves of Tetra-PEG gels. Using a three-component fit, we could quantify these distinct components with regards to their different residual dipolar coupling constants D_{res} and their weight fractions. We identified one component with a lower residual coupling (lower dynamic order parameters) compared to the single link with connectivity defects, i.e., double links between the macromonomers. The third component can be denoted as higher-order connectivity defects, yet its composition and distribution of order parameters are not measurable due to its complexity. This analysis is feasible because the Tetra-PEG gel is nearly free from larger-scale inhomogeneities, i.e., fixed concentration fluctuations. A verification of our assignment was taken from bond-fluctuation Monte Carlo simulations, which explicitly considered the cross-linking process of A−B tetra-arm star polymers. The main result of these simulations are the fractions of the network connectivity defects, which exhibit the same concentration-dependent trends as the experimental values.

In contrast to the previous light and neutron scattering studies[13,14,44] emphasizing the ideal and homogeneous nature of the Tetra-PEG gels, we could here refine this global statement by providing for the first time molecular-level information on the amounts of structural defects in these systems. These are considerable, indeed, and thus show that these systems, albeit being very homogeneous on the length scale beyond the mesh size, have a microstructure that is far from the ideal diamond-like structure that has been drawn in the first publications.[12,13] Strictly speaking, Tetra-PEG is thus not an "ideal" polymer network but certainly one of the most appealing model networks[43] available to the community. We expect that Tetra-PEG will be of use to tackle a number of open questions in the physics of polymer networks in the future.

AUTHOR INFORMATION

Corresponding Author

*E-mail: (F.L.) frank.lange@physik.uni-halle.de; (K.S.) kay.saalwaechter@physik.uni-halle.de.

Present Addresses

[%]Institut für Baustoffe, ETH Zürich, Schafmattstr. 6, 8093 Zürich, Switzerland.

ACKNOWLEDGMENT

Infrastructure support from the European Union (ERDF programme) is gratefully acknowledged.

REFERENCES

(1) Flory, P. J. *Principles of Polymer Chemistry*; Cornell University Press: Ithaca, NY, 1953.

(2) Paulino, A. T.; Guilherme, M. R.; Reis, A. V.; Gampese, G. M.; Muniz, E. C.; Nozaki., J. Removal of methylene blue dye from an aqueous media using superabsorbent hydrogel supported on modified polysaccharide. *J. Colloid Interface Sci.* **2006**, *301*, 55–62.

(3) Peppas, N. A.; Hilt, J. Z.; Khademhosseini, A.; Langer, R. Hydrogels in Biology and Medicine: From Molecular Principles to Bionanotechnology. *Adv. Mater.* **2006**, *18*, 1345–1360.

(4) Lee, K. Y.; Mooney, D. J. Hydrogels for Tissue Engineering. *Chem. Rev.* **2001**, *101*, 1869–1879.

(5) Tanaka, T. Phase transitions in gels and single polymer. *Polymer* **1979**, *20*, 1404–1412.

(6) Qiu, Y.; Park, K. Environment-sensitive hydrogels for drug delivery. *Adv. Drug Delivery Rev.* **2001**, *53*, 321–339.
(7) Harmon, M. E.; Tang, M.; Frank., C. W. A microfluidic actuator based on thermoresponsive hydrogels. *Polymer* **2003**, *44*, 4547–4556.
(8) Rouf, C.; Bastide, J.; Pujol, J. M.; Schlosseler, F.; Munch., J. P. Strain Effect on Quasistatic Fluctuations in a Polymer Gel. *Phys. Rev. Lett.* **1994**, *73*, 830–833.
(9) Mendes, E., Jr.; Lindner, P.; Buzier, M.; Boué, F.; Bastide, J. Experimental Evidence for Inhomogenious Swelling and Deformation in Statistical Gels. *Phys. Rev. Lett.* **1991**, *66*, 1595–1598.
(10) Bastide, J.; Leibler., L. Large-Scale Hetergeneities in Randomly Cross-Linked Networks. *Macromolecules* **1988**, *21*, 2647–2649.
(11) Lang, M.; Sommer, J.-U. On the origin of the scattering of gels and swollen polymer networks. *Const. Med. Rub.* **2007**, *5*, 147–156.
(12) Sakai, T.; Matsunaga, T.; Yamamoto, Y.; Ito, C.; Yoshida, R.; Suzuki, S.; Sasaki, N.; Shibayama, M.; Chung, U. Design and Fabrication of a High-Strength Hydrogel with Ideally Homogeneous Network Structure from Tetrahedron-like Macromonomers. *Macromolecules* **2008**, *41*, 5379–5384.
(13) Matsunaga, T.; Sakai, T.; Akagi, Y.; Chung, U.; Shibayama, M. Structure Characterization of Tetra-PEG Gel by Small-Angle Neutron Scattering. *Macromolecules* **2009**, *42*, 1344–1351.
(14) Matsunaga, T.; Sakai, T.; Akagi, Y.; Chung, U.; Shibayama, M. SANS and SLS Studies on Tetra-Arm PEG Gels in As-Prepared and Swollen States. *Macromolecules* **2009**, *42*, 6245–6252.
(15) Litvinov, V. M., De, P. P., Eds. *Spectroscopy of Rubbers and Rubbery Materials*; Rapra Technology Ltd.: Shawbury, 2002.
(16) Cohen-Addad, J. P.; Vogin, R. Molecular Motion Anisotropy as Reflected by a "Pseudosolid" Nuclear Spin Echo: Observation of Chain Constraints in Molten *cis*-1,4,-Polybutadiene. *Phys. Rev. Lett.* **1974**, *33*, 940–943.
(17) Sotta, P.; Fülber, C.; Demco, D. E.; Blümich, B.; Spiess, H. W. Effect of Residual Dipolar Interactions on the NMR Relaxation in Cross-Linked Elastomers. *Macromolecules* **1996**, *29*, 6222–6230.
(18) Sotta, P.; Deloche, B.; Herz, J.; Lapp, A.; Durand, D.; Rabadeux, J.-C. Evidence for Short-Range Orientational Couplings between Chain Segments in Strained Rubbers: A Deuterium Magnetic Resonance Investigation. *Macromolecules* **1987**, *20*, 2769–2774.
(19) Klein, P. G.; Adams, C. H.; Brereton, M. G.; Ries, M. E.; Nicholson, T. M.; Hutchings, L. R.; Richards., R. W. Rouse and Reptation Dynamics of Linear Polybutadiene Chains Studies by ^{2}H NMR Transverse Relaxation. *Macromolecules* **1998**, *31*, 8871–8877.
(20) Maxwell, R. S.; Chinn, S. C.; Solyom, D.; Cohenour., R. Radiation-Induced Cross-Linking in a Silica-Filled Silicone Elastomer As Investigated by Multiple Quantum ^{1}H NMR. *Macromolecules* **2005**, *38*, 7026–7032.
(21) Saalwächter, K. Proton Multiple-Quantum NMR for the Study of Chain Dynamics and Structural Constraints in Polymeric Soft Materials. *Prog. Nucl. Magn. Reson. Spectrosc.* **2007**, *51*, 1–35.
(22) Valentín, J. L.; Posadas, P.; Fernández-Torres, A.; Malmierca, M. A.; González, L.; Chassé, W.; Saalwächter., K. Inhomogeneities and Chain Dynamics in Diene Rubbers Vulcanized with Different Cure Systems. *Macromolecules* **2010**, *43*, 4210–4222.
(23) Saalwächter, K.; Kleinschmidt, F.; Sommer, J.-U. Swelling Heterogeneities in End-Linked Model Networks: A Combined Proton Multiple-Quantum NMR and Computer Simulation Study. *Macromolecules* **2004**, *37*, 8556–8568.
(24) Saalwächter, K.; Gottlieb, M.; Liu, R.; Oppermann, W. Gelation as Studied by Proton Multiple-Quantum NMR. *Macromolecules* **2007**, *40*, 1555–1561.
(25) Seiffert, S.; Oppermann, W.; Saalwächter, K. Hydrogel formation by photocrosslinking of dimethylmaleimide functionalized polyacrylamide. *Polymer* **2007**, *48*, 5599–5611.
(26) Sommer, J.-U.; Chassé, W.; Valentín, J. L.; Saalwächter, K. Effect of excluded volume on segmental orientation correlations in polymer chains. *Phys. Rev. E* **2008**, *78*, 051803.
(27) Valentín, J. L.; López, D.; Hernández, R.; Mijangos, C.; Saalwächter, K. Structure of Poly(vinyl alcohol) Cryo-Hydrogels as Studied by Proton Low-Field NMR Spectroscopy. *Macromolecules* **2009**, *42*, 263–272.
(28) Carmesin, I.; Kremer., K. The Bond Fluctuation Method: A New Effective Algorithm for the Dynamics of Polymers in All Spatial Dimensions. *Macromolecules* **1988**, *21*, 2819–2823.
(29) Deutsch, H. P.; Binder, K. Interdiffusion and self-diffusion in polymer mixtures: A Monte Carlo study. *J. Chem. Phys.* **1991**, *94*, 2294–2304.
(30) Lang, M.; Sommer, J.-U. Analysis of Entanglement Length and Segmental Order Parameter in Polymer Networks. *Phys. Rev. Lett.* **2010**, *104*, 177801.
(31) Sommer, J.-U.; Saalwächter, K. Segmental Order in Endlinked Polymer Networks: A Monte Carlo Study. *Eur. Phys. J. E* **2005**, *18*, 167–182.
(32) Chassé, W.; Valentín, J. L.; Genesky, G. D.; Saalwächter, K. Precise dipolar coupling constant distribution analysis in proton multiple-quantum NMR of elastomers. *J. Chem. Phys.* **2011**, *134*, 044907.
(33) Sommer, J.-U.; Schulz, M.; Trautenberg, H. Dynamical properties of randomly cross-linked polymer melts: A monte carlo study. i. diffusion dynamics. *J. Chem. Phys.* **1993**, *98*, 7515–7520.
(34) Trautenberg, H. L.; Sommer, J.-U.; Göritz, D. Structure and Swelling of End-linked Model Networks. *J. Chem. Soc., Faraday Trans.* **1995**, *91*, 2649–2653.
(35) Paul, W.; Binder, K.; Heermann, D. W.; Kremer, K. Crossover scaling in semidilute polymer solutions: a Monte Carlo test. *J. Phys. II* **1991**, *1*, 37–60.
(36) Schwenke, K.; Lang, M.; Sommer, J.-U. On the Structure of Star-Polymer Networks. *Macromolecules* **2011**, DOI: 10.1021/ma202022q.
(37) Akagi, Y.; Katashima, T.; Katsumoto, Y.; Fujii, K.; Matsunaga, T.; Chung, U.; Shibayama, M.; Sakai, T. Examination of the Theories of Rubber Elasticity Using an Ideal Polymer Network. *Macromolecules* **2011**, *44*, 5817–5821.
(38) Miller, D. R.; Macosko, C. W. A New Derivation of Post Gel Properties of Network Polymers. *Macromolecules* **1976**, *9*, 206–211.
(39) Parker, J. R. Simulated Annealing for Fitting Linear Combinations of Gaussians to Data. *Computing* **2000**, *65*, 291–312.
(40) James, H. M.; Guth, E. Simple Presentation of Network Theory of Rubber, with a Discussion of Other Theories. *J. Polym. Sci.* **1949**, *4*, 153–182.
(41) Rubinstein, M.; Colby, R. H. *Polymer Physics*; Oxford University Press: New York, 2003.
(42) Dušek, K.; Prins, W. Structure and Elasticity of Non-Crystalline Polymer Networks. *Adv. Polym. Sci.* **1969**, *6*, 1–102.
(43) Hild., G. Model Networks Based on 'Endlinking' Processes: Synthesis, Structure and Properties. *Prog. Polym. Sci.* **1998**, *23*, 1019–1149.
(44) Matsunaga, T.; Asai, H.; Akagi, Y.; Sakai, T.; Chung, U.; Shibayama., M. SANS Studies on Tetra-PEG Gel under Uniaxial Deformation. *Macromolecules* **2011**, *44*, 1203–1210.
(45) Lang, M.; Schwenke, K.; Sommer, J.-U. Rate Theory of Cyclic Structures in Polymer Model Networks. Manuscript in preparation.
(46) Lang, M.; Göritz, D.; Kreitmeier, S. Intramolecular Reactions in Randomly End-Linked Polymer Networks and Linear (Co)polymerizations. *Macromolecules* **2005**, *38*, 2515–2523.